Article:
Zhang, Menglong, Mitchell, Robert W., Huang, Haowei et al. (1 more author) (2017) Ordered multilayer films of hollow sphere aluminium-doped zinc oxide for photoelectrochemical solar energy conversion. Journal of Materials Chemistry A. pp. 22193-22198. ISSN: 2050-7496

https://doi.org/10.1039/c7ta07509j

Journal Name

ARTICLE

Ordered multilayer films of hollow sphere aluminium-doped zinc oxide for photoelectrochemical solar energy conversion

Received 00th January 20xx,
Accepted 00th January 20xx

DOI: 10.1039/x0xx00000x

www.rsc.org/

Menglong Zhang, Robert W. Mitchell, Haowei Huang, Richard E. Douthwaite*

Transparent conducting oxides (TCO's) are integral to many optoelectronic devices used for a range of display and solar energy technologies. Non-planar, 3-dimensional, TCO's offer the opportunity to support thin films of functional materials to increase light absorption, charge extraction, and wavelength-dependent manipulation of light if ordered into photonic structures. In addition increased surface area is also important for applications which rely on interfacial phenomena such as photoelectrochemical solar energy conversion, which is the focus of this investigation. Photoelectrodes have been fabricated from ordered spherical arrays of aluminium doped zinc oxide (AZO) and subsequently coated with photoactive semiconductor (CdS) nanoparticles using simple solution chemical deposition. The spheres of the structured AZO TCO are hollow and access to the internal volume supports loading of CdS as a thin film which results in increased light collection per geometric surface area. Efficient charge collection is observed, without restricting diffusion of electrolyte, allowing photocurrents ca. 20 times greater than a planar analogue.

Introduction

Transparent conducting oxide (TCO) films have wide application in display, solar cell and functional window technologies.[1-4] Furthermore, in addition to planar films, structured morphologies provide opportunities to improve or develop new applications dependent on surface area or light manipulation. These include photoelectrodes which are capable of converting solar-to-chemical energy and are commonly fabricated from TCO substrates covered with semiconducting photoactive materials. Photoelectrode efficiency is often compromised by a combination of limited light absorption, charge carrier recombination, and redox catalysis at the electrode/electrolyte interface. Improvements can be achieved by structuring the photoactive semiconductor. For example porous or nanoscale morphologies can increase photon absorption, improve charge collection, thus reducing recombination, and increase the electrode/electrolyte surface area.[5-8] However, fabrication of structured semiconductors is not always straightforward and is material dependent. An alternative is to use a structured TCO and coat the surface with a film of photoactive semiconductor using simple methods such as dip-coating or vapor deposition applicable to a wide range of materials. Indium tin oxide (ITO) dominates the TCO field, however the supply and cost of indium oxide has prompted the investigation of alternative materials, principally tin and zinc oxides.[2, 3, 9] Aluminium-doped zinc oxide (AZO) has been of particular interest due to the earth abundance and lower environmental impact compared to heavier metals.[2, 10] Hollow nanostructures, particularly spheres of metal oxides have also been of great interest for numerous applications in catalysis, gas sensing and battery technologies, because such structures can exhibit high surface area and support rapid transport of molecules and ions. However, an outstanding challenge is to fabricate ordered 3-dimensional arrays to improve transport properties and open up new opportunities in optical applications. We were motivated to explore the preparation of ordered films of hollow spheres of a TCO such as AZO for photoelectrochemical applications. Undoped ZnO microspheres that have been used as powders for photocatalysis,[11-16] and as disordered supports for dye-sensitized solar cells,[5, 17-20] gas sensors[21-23] and media for Li-ion batteries.[24] In addition, monolayers of ordered arrays of ZnO urchin-like structures derived from nanorods have been reported.[25] However, ordered hollow sphere arrays of a TCO have not been reported.

Herein, we describe the synthesis of 3-dimensional structured films of AZO comprising ordered multilayers of porous hollow spheres (hs-AZO). The hs-AZO films allow diffusion of liquid which supports simple solution deposition of semiconductor films and access to electrolyte for photoelectrochemical applications. For example, coating CdS semiconductor gives photoelectrodes that can support current densities ca. 20 times that of planar analogues.

[a] Department of Chemistry, University of York, Heslington, York, YO10 5DD (UK). E-mail: richard.douthwaite@york.ac.uk
Electronic Supplementary Information (ESI) available: [details of any supplementary information available should be included here]. See DOI: 10.1039/x0xx00000x

Experimental

Materials

H_2SO_4 (≥ 95 %), $H_2O_{2(aq)}$ (30 v%), CdO (99.99 %), oleic acid (99 %), octadecene (90 %), sulphur (99 %), $Na_2S.9H_2O$ (98 %), Na_2SO_3 (98 %), $AlCl_3$ (99.99 %), $Zn(Ac)_2.2H_2O$ (98 %), KCl (99 %), FTO glass (7 Ω/sq), ethanol and toluene were purchased from Sigma Aldrich and used as received. Polystyrene sphere template (450 nm diameter) was prepared using a literature method.[26]

Fabrication of polystyrene film template

FTO coated electrodes (2 x 10 x 15 mm) were soaked in piranha solution (3:1 H_2SO_4:H_2O_2) for 2 hours before being washed with deionised water and dried under N_2. Typically, an electrode was stood vertically in a glass vial containing a suspension of polystyrene spheres (PS) dispersed in ethanol and water (1:82:8 PS:ethanol:water) to a level just above the top of the electrode. The volatiles were evaporated over 15 h at 60 ˚C until 10 mm of film was deposited. The electrode was then removed and the remaining 5 mm cleaned with acetone giving an electrode coated in a continuous opalescent polystyrene film 10 x 10 mm and *ca*. 7 -10 μm thick.

Synthesis of hs-AZO film

AZO precursor was prepared from $Zn(Ac)_2.2H_2O$ (2 g, 9.1 mmol) dissolved in 40 mL of methanol with sonication until clear. To this solution $AlCl_3$ (8 mg, 0.06 mmol) was then added and the solution sonicated for 1 h and used immediately. The PS template was soaked in methanol for 30 min before being stood vertically and submerged in the AZO solution (3.5 mL) in a glass vial and stored in a desiccator under reduced pressure for 1 hr. The soaked PS film was removed from the vial and then calcined at 450 ^{o}C for 2 hr with a heat ramp rate of 1 ^{o}C min^{-1} to give an hs-AZO film.

Coating of hs-AZO with CdS

An hs-AZO electrode was stood vertically in a glass vial containing a solution of 50 mM $Cd(Ac)_2$ in ethanol (3 mL)) for 1 min and then dried under a stream of nitrogen. The electrode was then stood vertically in a second glass vial containing a 50 mM $Na_2S_{(aq)}$ (3 mL) for 1 min, rinsed with distilled water and dried under a stream of nitrogen. The process was repeated 5 times to give the optimized photocurrent. The electrode was finally heated under argon at 400 ^{o}C using a ramp rate of 1 ^{o}C min^{-1} and held for 30 min until an orange electrode was obtained.

Characterisation

SEM images were obtained using an FEI Sirion scanning electron microscope. Energy Dispersive Analysis of X-rays (EDX) was performed using an attached EDAX Phoenix X-ray spectrometer. Electrodes were stuck to an aluminium stub using carbon sticky tape. TEM images were obtained using a JEOL 2011 transmission electron microscope operated at 200 kV accelerating voltage. Samples were scraped off the FTO glass substrate, then ground in methanol and sonicated for 15 mins. One drop of the dispersion was deposited onto 3 mm holey carbon coated copper grids and allowed to dry in air. Particle size distributions of nanoparticles were evaluated by averaging the diameter of > 100 particles from TEM images. Diffuse reflectance UV-vis spectra were recorded on an Ocean Optics HR2000+ High Resolution Spectrometer with DH-2000-BAL Deuterium/Helium light source (200-1100 nm) and a R400-7-UV-Vis reflection probe at an incidence angle of 45^{o}. Spectra were recorded in Spectra Suite software using an integration time of 10 seconds, box car smoothing width of 30, and 10 scans to average. Wide angle PXRD patterns were recorded on a Bruker-AXS D8 Advance instrument with Lynx eye detector, using Cu Kα radiation (1.54 Å) with a 1 mm slit on the source and 2.5 mm detector slit. Data was collected from 10 – 70 ° 2θ, with 0.02 ° step size and a scan speed of 0.1 seconds per step. Samples were deposited as films on an aluminium sample holder. Sheet resistances were determined using a home-made apparatus via the Van der Pauw method. The four point probes were in a square configuration and contact was made via spring-loaded gold screws.

Electrochemical measurements were made using a standard 3 electrode setup. The reference electrode was Ag/AgCl (3 M NaCl internal solution), and a platinum wire was used as the counter electrode. Connection to the FTO working electrode was achieved using copper tape and the bottom 10 mm of the electrode was immersed in the electrolyte solution. The photoelectrochemical cell contained a Pyrex window (15 mm diameter) through which the sample was illuminated using a 150 W Xe lamp with irradiance of ca. 100 $mWcm^{-2}$. Electrolyte solutions of aqueous Na_2S/Na_2SO_3 (0.25/0.35 M) were prepared using water filtered through a Millipore system (> 18 MΩ cm^{-3}), and degassed for 10 mins with N_2 before use. All potentials are referenced to the reversible hydrogen electrode using the following equation.

$$E_{RHE} = E_{vs\ Ag/AgCl} + E_{ref(Ag/AgCl)} + 0.059pH$$

Where $E_{ref(Ag/AgCl)}$ = 0.209 V vs NHE at 25 ^{o}C. Electrochemical impedance spectroscopy was performed using a Biologic SP-150 potentiostat between 10 kHz and 10 mHz at an amplitude of ±10 mV using the same configuration as for photoelectrochemical measurements. Data was fit to equivalent circuits using the Z Fit function within EC-Lab software. Incident Photon-to-Electron Efficiency (IPCE) was measured over 350 – 600 nm and calculated using the following equation.

$$\mathrm{IPCE} = \frac{1238.9\ \left(\mathrm{W}.\frac{\mathrm{nm}}{\mathrm{A}}\right) \times j\left(\frac{\mathrm{mA}}{cm^2}\right)}{\lambda(\mathrm{nm}) \times E_e\left(\frac{\mathrm{mW}}{cm^2}\right)}$$

Where j is the measured photocurrent density, λ is the wavelength of incident light, Ee is the measured irradiance at the wavelength λ. The irradiance was measured using a

certified International Light Technologies 1400-A Radiometer Photometer.

Results and Discussion

Synthesis and characterization of hollow sphere AZO films

Films of hs-AZO were fabricated using a soft templating technique, by addition of AZO precursor solution to an ordered array of monodisperse polystyrene spheres. The template spheres deposit as an fcc array (Fig. 1a) typically 5 μm thick which are then soaked in an AZO precursor solution under reduced pressure to encourage maximal filling of the template. Filling is sensitive to precursor viscosity and soaking time and we found that the morphology of the final film is also sensitive to the Al concentration. Al precursor contents above ca. 1 at % did not lead to effective filling due to increased viscosity and below ca. 0.3 at % the more common inverse opal structures typical of undoped ZnO were observed.[27] Soaking for 1 h with an Al 0.4 at % solution was found to be optimum with incomplete filling observed after shorter soaking times (Fig. S1a, Supplementary Information). Template removal occurs on calcination in air to give films that show a spherical motif of ca. 400 nm with a close packed fcc structure (Fig. 1b). Comparison of the scanning electron microscopy (SEM) images of the template (Fig. 1a) and hs-AZO (Fig. 1b and c) films both show a spherical motif of ca. 400 nm with a close packed fcc structure, with coverage extending over large areas replicating the opal template structure. The internal structure is evident after scratching the surface of an hs-AZO film showing that the spheres are hollow with walls ca. 35 nm thick (Fig. 1d). The hs-AZO films are ca. 3 - 5 μm thick randomly distributed across the film, which corresponds to 8 - 12 layers (Fig 1e) and is reflective of variability in the template film thickness. Each sphere is composed of agglomerations of nanoparticles 5 - 20 nm in diameter (Fig. 1f) with voids between the agglomerations giving a rough appearance (Fig. S1b).

The aluminium content of hs-AZO was determined by energy dispersive analysis of x-rays (EDX) indicating doping of 1.0 at % (Fig. S2), which is greater than that present in the precursor solution and presumably due to the lower solubility of aluminium oxides. Powder X-ray diffraction (PXRD) (Fig. S3) gives peaks consistent with the wurtzite phase of ZnO and reported examples of planar AZO films.[28]

An ordered array of 400 nm spheres will result in a periodic modulation of the refractive index likely leading to photonic behavior. This is manifested as wavelength dependent propagation of light which can be most simply demonstrated using diffuse reflectance UV-vis spectroscopy (DRUVS).[29] A characteristic peak (stop band) is observed for wavelengths with modified propagation resulting in reflection at the stop band maximum (λ_{max}). Eqn. 1 and 2 describe the relationship between λ_{max} and the relative refractive indices (n) of the void and wall materials, lattice plane spacing (d_{hkl}), volume wall fill factor (φ), Bragg plane order (m), angle of incidence (θ), and the lattice periodicity (D).[29]

$$\lambda_{\max} = \frac{2d_{hkl}}{m}[\varphi n_{wall}^2 + (1-\varphi)n_{\text{void}}^2 - \sin^2\theta]^{1/2} \quad (1)$$

$$d_{\text{hkl}} = \frac{D\sqrt{2}}{\sqrt{h^2+l^2+k^2}} \quad (2)$$

DRUVS of hs-AZO (Fig. 2) in air shows a broad stop band reflection at λ_{max} = 530 nm which allows a fill factor to be calculated based on n_{ZnO} = 1.9,[30] n_{air} = 1.0, m = 1, D = 400 nm (from SEM), and θ = 45 ^{o} giving φ = 6.1 %. The value of φ indicates that the film is primarily void and the broad width of the stop band is indicative of the structural imperfection arising from the agglomeration of nanoparticles (Fig. 1e) which define the spheres. SEM and TEM (Fig. 1e and 1f) indicate that the surface of the spheres comprises rough agglomerates and the spheres are porous. The accessibility of the inner volume of the film is important for applications such as photoelectrochemistry and can be conveniently probed using DRUVS. The stop band position and intensity in the DRUVS spectrum will be modified on exchange of air for a material of different refractive index. On addition of water (n = 1.33) or ethanol (n = 1.36) both showed complete suppression of the stop band (Fig. 2), indicating replacement of the air volume within the spheres. Suppression, rather than a red shift expected from Equation 1, occurs due to some trapped air

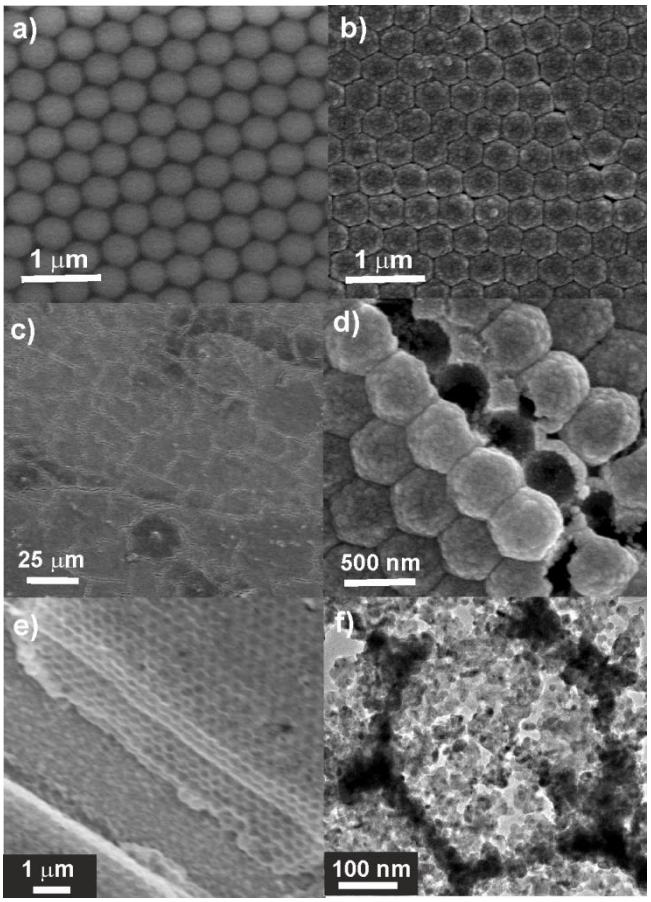

Fig. 1. SEM images a - e) showing a) polystyrene template; b) hs-AZO on same scale as a); c) larger area coverage; d) fractured region showing hollow interior; e) crack region showing a cross section of the hs-AZO film; f) TEM of hs-AZO.

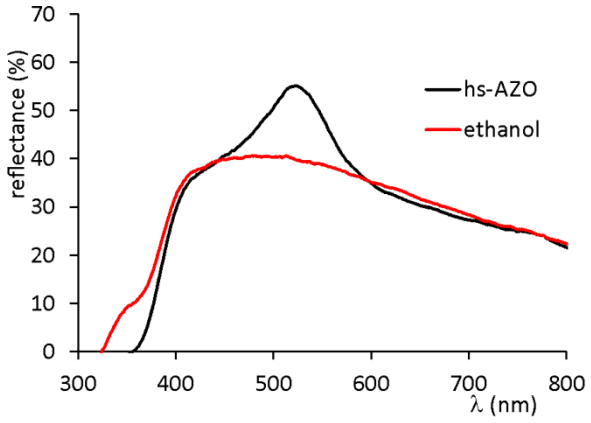

Fig. 2. DRUVS spectra of hs-AZO filled with air and ethanol.

bubbles and smaller refractive index difference between hs-AZO and water compared to air. On drying the films the DRUVS data before and after exposure to water and ethanol are indistinguishable. For ethanol the stop band returns within 3 min at room temperature indicating that diffusion in and out of the internal volume is rapid.

Transmission spectroscopy (Fig. S5) shows that the roughness of the films also gives rise to scattering in the visible range with an average transmittance of 40 % between 400 and 900 nm. The sheet resistance using four point probe measurements is ca. 8 Ω/□, which is typical of TCO type materials. However, it should be noted that a conductive substrate is required or the resistance is two orders of magnitude greater due to the grain boundaries and reduced contacts compared to a condensed planar film. Conductivity across the film is therefore mediated perpendicular to the film via the conductive substrate.

Coating of hs-AZO with CdS

Given that the inner volume of the hs-AZO films is accessible to a liquid, solution deposition of a photoactive semiconductor was investigated for a photoelectrochemical study. CdS has been extensively investigated as a photoactive material and can be deposited on substrates via various methods for photoelectrochemical and quantum dot solar cell technology In related work these include CdS addition to various morphologies of ZnO based films, including nanorod, nanotube, nanocone, nanocable and macroporous morphologies.[31-38] Here, in situ deposition was achieved by soaking hs-AZO in aqueous solutions of $Cd(Ac)_2$ and NaS sequentially, which can be repeated to control the thickness of the coating. SEM of CdS@hs-AZO (Fig. 3a) shows a similar morphology to hs-AZO but with reduced surface roughness which is also evident in the interior of the spheres (Fig. 3b) indicating internal coverage by CdS. TEM (Fig. 3c) shows lattice fringes consistent with CdS and a particle size of ca. 10 nm. EDX mapping (Fig. 3d) shows that CdS is homogeneous across the electrode surface. Peaks consistent with CdS are also observed in PXRD data (Fig. S4).

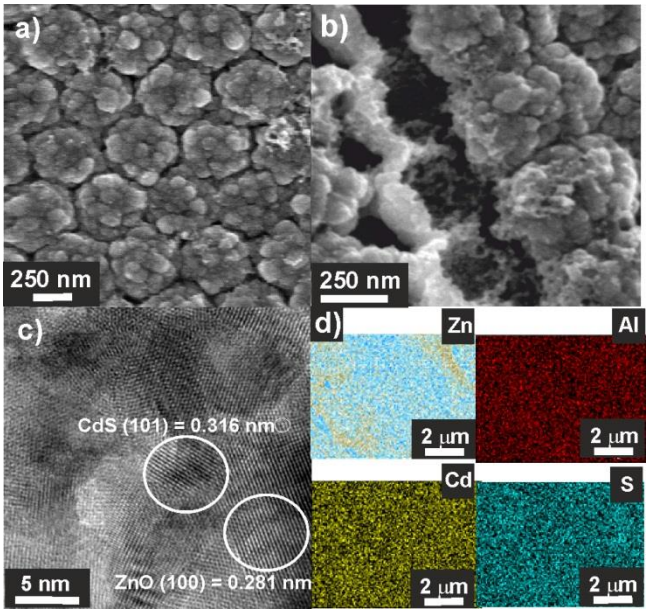

Fig. 3. a) SEM image of CdS@hs-AZO; b) SEM of a fractured region of CdS@hs-AZO; c) TEM image of CdS@hs-AZO showing lattice fringes of CdS and ZnO particles; d) EDX maps showing coverage of Zn, Al, Cd and S.

DRUVS (Fig. 4) shows the onset of absorption at ca. 520 nm consistent with the band gap of CdS (2.4 eV) and a weak stop band at 555 nm. For an electrode coated with 5 deposition cycles of CdS a red shift of 25 nm is observed. Equation 1 can be modified to include an additional component, χ, which corresponds to the volume fraction of CdS (Eqn. 3).[26] After 5 deposition cycles λ_{MAX} = 555 nm, *D* = 400 nm, m = 1, n_{AZO} = 1.9, n_{air} = 1, n_{CdS} = 2.4,[30] φ = 0.061 (6.1 %) allowing a calculated estimate of χ_{CdS} = 1.3 % which compares to 6.1 % for the hs-AZO support and is broadly consistent with the SEM images (Fig. 1d and 3b).

$$\lambda_{\max} = \frac{2d_{hkl}}{m}\left[\varphi n_{wall}^2 + \chi n_{\mathrm{CdS}}^2 + (1-\varphi-\chi)n_{\mathrm{void}}^2 - \sin^2\theta\right]^{\frac{1}{2}} \quad (3)$$

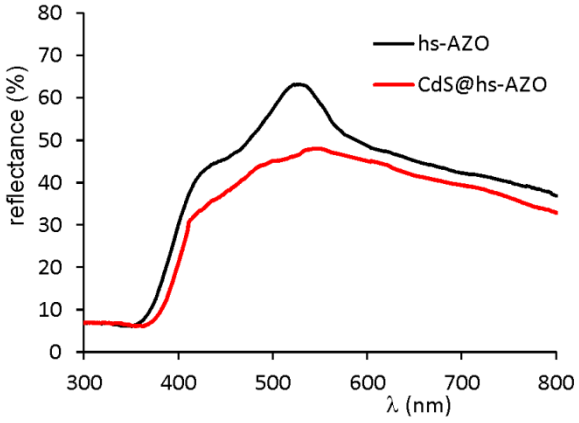

Fig. 4. DRUVS data for hs-AZO and CdS@hs-AZO in air.

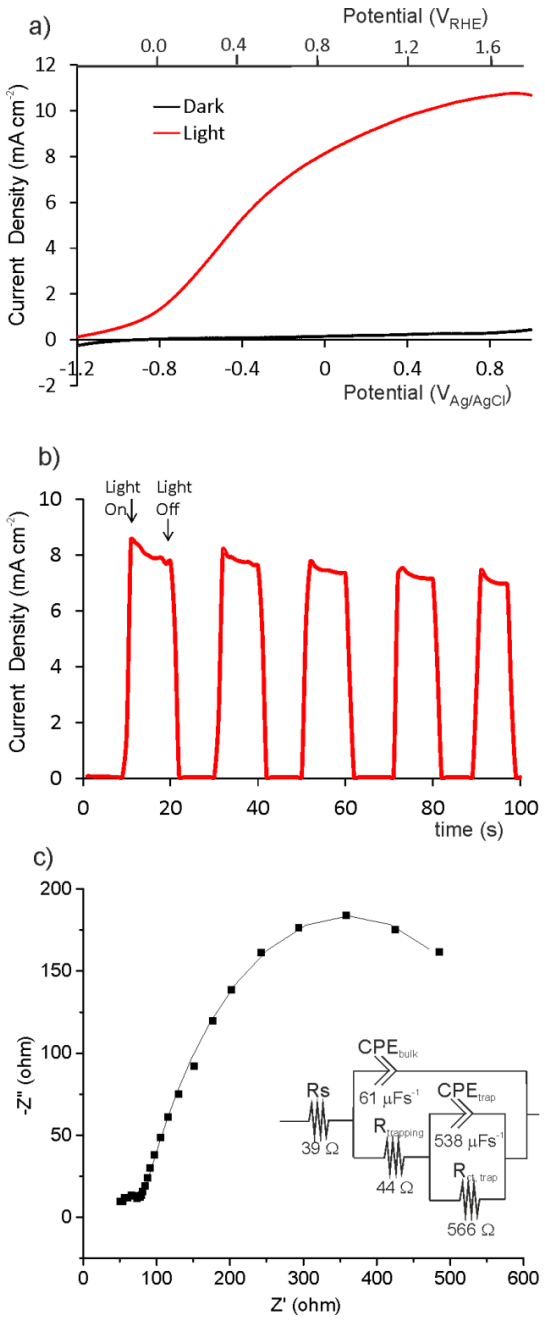

Fig. 5. CdS@hs-AZO (5 CdS deposition cycles); a) Linear sweep voltammogram; b) chronoamperometry at 0 V vs Ag/AgCl, 100 mWcm^{-2}; c) Electrochemical impedance spectrum (Nyquist plot) at 0 V vs Ag/AgCl, 100 mWcm^{-2}, where the line is the fit to the circuit shown.

Photoelectrochemistry of CdS@hs-AZO was performed in an aqueous electrolyte containing Na_2S (0.25 M)/Na_2SO_3 (0.35 M) under illumination with a Xe light source of irradiance 100 mWcm^{-2}. Linear sweep voltammetry, at 10 mVs^{-1}, shows that CdS@hs-AZO electrodes exhibit a significant photoresponse (Fig. 5a) strongly indicating that addition of CdS does not prevent electrolyte penetrating the hs-AZO film. The photocurrent density is maximized at 5 deposition cycles and begins to decrease after 7 cycles (Fig. S8). Chronoamperometry at 0 V vs Ag/AgCl (Fig. 5b) of CdS@hs-AZO exhibits a maximum photocurrent of ca. 8.0 mA cm^{-2} indicating that light collection and charge separation are very efficient, in addition to essentially unrestricted electrolyte diffusion through the hollow sphere structure. This is in comparison to 0.4 mA cm^{-2} for CdS on a planar substrate and 5.0 mA cm^{-2} for CdS on AZO nanorod arrays, respectively measured under similar conditions.[36] Photostability is similar to other CdS systems in Na_2S/Na_2SO_3 electrolyte, which reduces photocorrosion, and exhibits an initial reduction over minutes followed by a plateau (Fig. S9).[35, 36]

Charge transport properties of the photoelectrodes were examined using electrochemical impedance spectroscopy (EIS) which was performed under illumination between 10 mHz and 10 kHz. The Nyquist plot (Fig. 5c) shows a semi-circular feature at high frequencies and a larger radius feature at lower frequencies. These data can be fit to an equivalent circuit (Fig. 5c inset) that have been applied to metal oxide photoelectrodes that are interpreted physiochemically as resistive and capacitive elements arising from bulk trapping and charge transfer from intraband trap states.[39] The magnitude of the resistive elements ranging from ca 40 to 550 Ω is comparable to planar films of CdS on conducting substrates. These data indicate that charge carrier mobility across the film and at the electrode/electrolyte interface is not significantly modified by the hs-AZO structure and that collection occurs throughout the bulk of the film, with unrestricted passage of electrolyte.

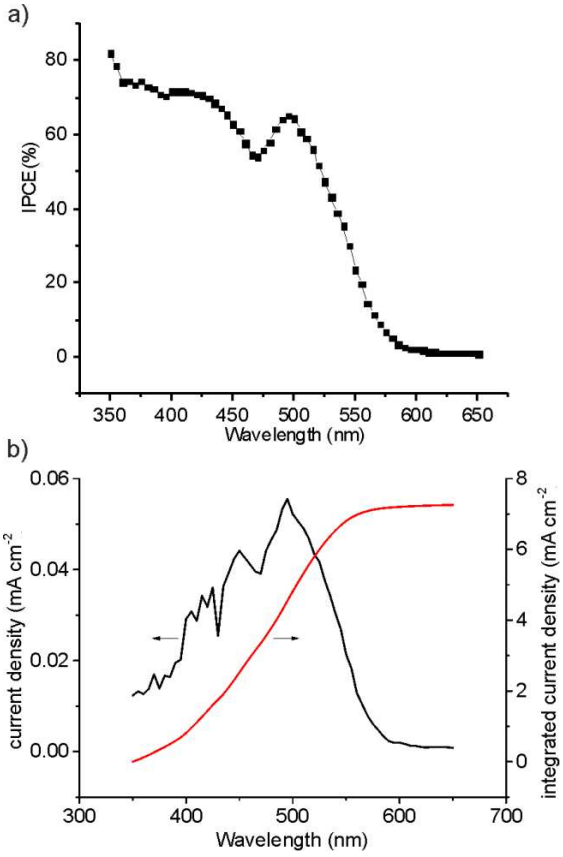

Fig. 6. CdS@hs-AZO (5 CdS deposition cycles); a) IPCE measurements obtained at 0 V vs Ag/AgCl; b) Current density and integrated current density as a function of wavelength.

Incident photon-to-current efficiency (IPCE) measurements (Fig. 6a) were performed between 350 and 600 nm at 0 V vs Ag/AgCl to investigate the wavelength dependence of the photoresponse. The profile is consistent with the absorption spectrum of CdS indicating that hs-AZO is not a significant absorber. Commonly the IPCE of shorter wavelengths is reduced due to reflection and lower light penetration depth. The IPCE observed here indicates that hs-AZO efficientlymediates charge collection via support of a thin film of CdS particles and the hollow-sphere morphology limits reflection. Calculation of the integrated current density based on the IPCE and Xe irradiance as a function of wavelength (Fig. 5a) gave density between 350-650 nm = 7.26 mA cm-2 which is comparable to that measured under broad band illumination (Fig. 6b).

Conclusions

Incorporation of an AZO precursor into a polystyrene template is sufficient to generate ordered hollow spheres that form over large areas with limited cracking. Simple solution methodology can be used to coat materials throughout the film including the internal surface area, without subsequently restricting access of liquid to the internal volume of the film. Coating with a photoactive semiconductor gives photoelectrodes that can support high current density due to the volume of semiconductor that can be supported on the structured electrode and internal light scattering, whilst retaining efficient charge extraction and unrestricted diffusion of electrolyte throughout the film.

Conflicts of interest

There are no conflicts to declare.

Acknowledgements

The authors thank the Wild Fund (M.Z. and H.H.) and University of York for generous financial support.

References

1. K. Ellmer, *Nat. Photonics*, 2012, **6**, 808-816.
2. S. C. Dixon, D. O. Scanlon, C. J. Carmalt and I. P. Parkin, *J. Mater. Chem. C*, 2016, **4**, 6946-6961.
3. K. H. L. Zhang, K. Xi, M. G. Blamire and R. G. Egdell, *J. Phys. Condens. Mat.*, 2016, **28**, 19.
4. X. G. Yu, T. J. Marks and A. Facchetti, *Nat. Mater.*, 2016, **15**, 383-396.
5. H. N. Chen and S. H. Yang, *Nanoscale Horiz.*, 2016, **1**, 96-108.
6. F. E. Osterloh, *Chem. Soc. Rev.*, 2013, **42**, 2294-2320.
7. H. G. Park and J. K. Holt, *Energy Environ. Sci.*, 2010, **3**, 1028-1036.
8. P. V. Kamat, *J. Phys. Chem. C*, 2007, **111**, 2834-2860.
9. C. Klingshirn, *Chemphyschem*, 2007, **8**, 782-803.
10. A. B. Djurisic, X. Liu and Y. H. Leung, *Phys. Status Solidi R.*, 2014, **8**, 123-132.
11. H. J. Wu, G. L. Wu, Y. Y. Ren, X. H. Li and L. D. Wang, *Chem. Eur. J.*, 2016, **22**, 8864-8871.
12. X. Wang, M. Y. Liao, Y. T. Zhong, J. Y. Zheng, W. Tian, T. Y. Zhai, C. Y. Zhi, Y. Ma, J. N. A. Yao, Y. Bando and D. Golberg, *Adv. Mater.*, 2012, **24**, 3421-3425.
13. T. Gordon, M. Kopel, J. Grinblat, E. Banin and S. Margel, *J. Mater. Chem.*, 2012, **22**, 3614-3623.
14. C. Q. Zhu, B. A. Lu, Q. Su, E. Q. Xie and W. Lan, *Nanoscale*, 2012, **4**, 3060-3064.
15. Z. W. Deng, M. Chen, G. X. Gu and L. M. Wu, *J. Phys. Chem. B*, 2008, **112**, 16-22.
16. J. G. Yu and X. X. Yu, *Environ. Sci. Technol.*, 2008, **42**, 4902-4907.
17. D. Xiang, F. Y. Qu, X. Chen, Z. Yu, L. R. Cui, X. Zhang, J. J. Jiang and H. M. Lin, *J. Sol-Gel Sci. Technol.*, 2014, **69**, 370-377.
18. Z. H. Dong, X. Y. Lai, J. E. Halpert, N. L. Yang, L. X. Yi, J. Zhai, D. Wang, Z. Y. Tang and L. Jiang, *Adv. Mater.*, 2012, **24**, 1046-1049.
19. X. J. Lu, F. Q. Huang, X. L. Mou, Y. M. Wang and F. F. Xu, *Adv. Mater.*, 2010, **22**, 3719-3722.
20. R. R. Bacsa, J. Dexpert-Ghys, M. Verelst, A. Falqui, B. Machado, W. S. Bacsa, P. Chen, S. M. Zakeeruddin, M. Graetzel and P. Serp, *Adv. Funct. Mater.*, 2009, **19**, 875-886.
21. S. Li, M. Chen and X. D. Liu, *Opt. Express*, 2014, **22**, 18707-18714.
22. K. Matsuyama, K. Mishima, T. Kato and K. Ohara, *Ind. Eng. Chem. Res.*, 2010, **49**, 8510-8517.
23. J. Zhang, S. Wang, Y. Wang, M. Xu, H. Xia, S. Zhang, W. Huang, X. Guo and S. Wu, *Sens. Actuators, B*, 2009, **139**, 411-417.
24. F. Q. Liu, H. M. Wu, T. Li, L. R. Grabstanowicz, K. Amine and T. Xu, *Nanoscale*, 2013, **5**, 6422-6429.
25. J. Elias, C. Levy-Clement, M. Bechelany, J. Michler, G. Y. Wang, Z. Wang and L. Philippe, *Adv. Mater.*, 2010, **22**, 1607-1612.
26. R. Mitchell, R. Brydson and R. E. Douthwaite, *Nanoscale*, 2014, **6**, 4043-4046.
27. A. Stein, B. E. Wilson and S. G. Rudisill, *Chem. Soc. Rev.*, 2013, **42**, 2763-2803.
28. W. Tang and D. C. Cameron, *Thin Solid Films*, 1994, **238**, 83-87.
29. R. C. Schroden, M. Al-Daous, C. F. Blanford and A. Stein, *Chem. Mat.*, 2002, **14**, 3305-3315.
30. D. R. Lide, *CRC Handbook of Chemistry and Physics*, CRC Press, Boca Raton, FL, 76th edn., 1996.
31. N. M. Vuong, J. L. Reynolds, E. Conte and Y. I. Lee, *J. Phys. Chem. C*, 2015, **119**, 24323-24331.
32. H. Liu, G. M. Zhang, J. B. Yin, J. Liang, W. T. Sun and Z. Y. Shen, *Mater. Res. Bull.*, 2015, **61**, 492-498.
33. J. P. Deng, M. Q. Wang, J. Liu, X. H. Song and Z. Yang, *J. Colloid Interface Sci.*, 2014, **418**, 277-282.
34. H. N. Hieu, N. M. Vuong and D. Kim, *J. Electrochem. Soc.*, 2013, **160**, H852-H857.
35. X. P. Qi, G. W. She, Y. Y. Liu, L. X. Mu and W. S. Shi, *Chem. Commun.*, 2012, **48**, 242-244.
36. C. H. Hsu and D. H. Chen, *Nanoscale Res. Lett.*, 2012, **7**, 11.

37. G. Guerguerian, F. Elhordoy, C. J. Pereyra, R. E. Marotti, F. Martin, D. Leinen, J. R. Ramos-Barrado and E. A. Dalchiele, *Nanotechnology*, 2011, **22**, 9.
38. Y. Tak, S. J. Hong, J. S. Lee and K. Yong, *J. Mater. Chem.*, 2009, **19**, 5945-5951.
39. B. Klahr, S. Gimenez, F. Fabregat-Santiago, T. Hamann and J. Bisquert, *J. Am. Chem. Soc.*, 2012, **134**, 4294-4302.